Chinese Journal of
POLYMER SCIENCE

RESEARCH ARTICLE

https://doi.org/10.1007/s10118-026-3703-9
Chinese J. Polym. Sci.

End-to-End Neuron-inspired Signal Transduction Using Organic Electrochemical Transistors

Jin-Yao Wang[a,b,c], Yue Tian[a,b,c], Yi-Fan Xie[a,b,c], Miao Cheng[a,b,c], Chang-Rui Liu[a,b,c], Jing-Yun Chu[a,b,c], Guo-Qing Xie[a,b,c], Neng Gao[a,b,c], Hao-Fan He[a,b,c], Le-Jing Huang[a,b,c], Ling-Fei Wang[a,b,c], and Meng-Meng Li[a,b,c*]

[a] *Institute of Microelectronics, Chinese Academy of Sciences, Beijing 100029, China*
[b] *School of Integrated Circuits, University of Chinese Academy of Sciences, Beijing 100049, China*
[c] *State Key Laboratory of Fabrication Technologies for Integrated Circuits, Chinese Academy of Sciences, Beijing 100029, China*

Electronic Supplementary Information

Abstract Organic electrochemical transistors (OECTs) enable high-performance bioelectronics through their efficient ionic-electronic coupling, yet realizing a complete neuronal signal pathway that transduces environmental stimuli into spiking activity and synaptic memory remains a persistent system-level challenge. Here we demonstrate a neuron-inspired signal transduction pathway constructed entirely from OECTs, comprising a signal receptor, a spiking axonal module and a synaptic memory unit. System-level functionality is examined using a hardware-in-the-loop configuration based on direct analog signal transfer. The raw output photocurrent generated by the receptor drives the axonal oscillator, and the resulting voltage spikes subsequently modulate the synaptic device, without any algorithmic scaling or software-based amplification. This direct-drive regime preserves physical signal causality and reveals that the intrinsic signal levels of each functional block are naturally matched to the input requirements of the subsequent stage. Experimentally, receptor-induced spiking activity reliably gives rise to short-term synaptic plasticity under these unassisted conditions. Together, these results demonstrate the inherent inter-stage electrical compatibility of OECT-based devices and establish a rigorous experimental foundation for the future monolithic integration of fully organic neuromorphic systems.

Keywords Organic electrochemical transistors; Artificial neuron; Signal transduction; Hardware-in-the-loop configuration

Citation: Wang, J. Y.; Tian, Y.; Xie, Y. F.; Cheng, M.; Liu, C. R.; Chu, J. Y.; Xie, G. Q.; Gao, N.; He, H. F.; Huang, L. J.; Wang, L. F.; Li, M. M. End-to-end neuron-inspired signal transduction using organic electrochemical transistors. *Chinese J. Polym. Sci.* https://doi.org/10.1007/s10118-026-3703-9

INTRODUCTION

Traditional electronic systems and biological neural tissues are fundamentally mismatched in signal transduction and physicochemical properties[1] resulting in low signal translation efficiency, poor information fidelity, and limited long-term compatibility at heterogeneous interfaces, which are major obstacles for neural engineering and brain-computer interfaces. Artificial neurons have emerged to bridge this gap by mimicking the core electrophysiological features of biological neurons, generating action potential-like signals with biologically relevant amplitudes and timescales, while reproducing key dynamic processes such as synaptic weight modulation and firing adaptation.[2–6] However, conventional silicon-based metal-oxide-semiconductor field-effect transistors (MOSFETs) face intrinsic limitations in replicating these functions; they rely on electron conduction rather than ionic signaling, are typically rigid and mechanically incompatible with soft tissues, and operate at voltage and power levels far exceeding those of biological neurons.[7,8] Consequently, MOSFET-based circuits struggle to achieve long-term, high-fidelity, and low-damage interactions with living neural systems. In contrast, organic electrochemical transistors (OECTs) regulate channel conductivity through ion doping/dedoping, operate at low voltages with biologically comparable power consumption, and can be fabricated from flexible and biocompatible materials.[5,9] These features allow OECTs to emulate action potentials and synaptic dynamics while achieving high physical and functional biomimicry, providing a versatile hardware platform for seamless neural interfaces.[10,11]

As the fundamental structural and functional unit of the nervous system, a classical neuron comprises three interdependent regions that mediate reception, integration, conduction, and transmission of neural signals (Fig. 1).[12,13] The signal reception zone, formed by dendrites and the cell body, converts chemical or electrical inputs into local membrane potentials that are integrated over space and time.[14,15] The axon serves as the signal encoding and conduction pathway. When depolarization surpasses a threshold, voltage-gated ion channels generate all-or-none action potentials, enabling long-distance, high-fidelity transmission.[16,17] The synapse, as the third region, forms specialized junctions that regulate signaling and provide a physical basis for memory *via* synaptic

* Corresponding author, E-mail: limengmeng@ucas.ac.cn
Invited Research Article
Received February 26, 2026; Accepted April 4, 2026; Published online July 9, 2026

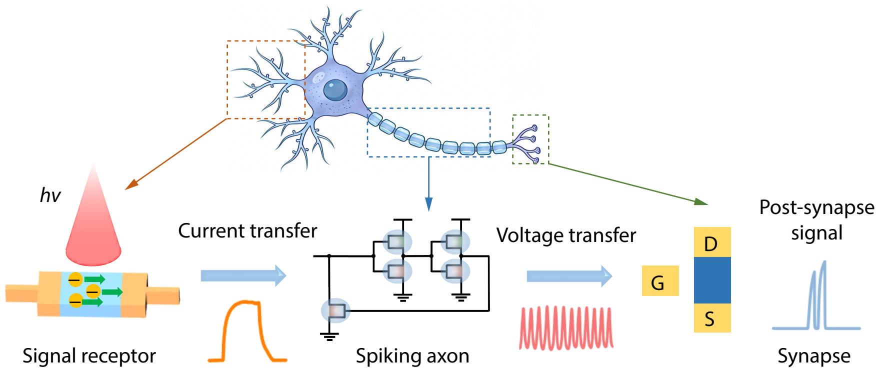

Fig. 1 The implementation pathway of OECT artificial neurons.

plasticity.[18,19] In artificial neurons constructed from OECTs, discrete studies have demonstrated biomimetic functionality within each of these regions, and the Inal group employed a retina-inspired p-type ion-optoelectronic synaptic OECT to achieve simultaneous light perception and adaptive modulation across the visible-to-near-infrared spectrum.[20] Rivnay's group realized tunable threshold spiking neurons with vertical anti-ambipolar bilayer OECTs, enabling precise control of firing.[21] Lee's group enhanced short- and long-term synaptic plasticity using amino-silane-modified P3HT OECTs, improving the conductance stability by promoting crystalline aggregation.[22] Despite these advances, constructing a fully integrated, monolithic artificial neuron remains challenging, and variations in ion dynamics and operational timing between functional modules can lead to signal distortion or delay, whereas reliance on external passive components such as discrete capacitors hinders high-density integration and overall system performance.[21−23] Addressing these interrelated challenges is essential for advancing discrete demonstrations to compact, fully integrated OECT-based neuromorphic systems.[6]

This study presents a functionally complete neuromorphic neuron architecture that implements end-to-end neuron-inspired signal transduction entirely using photolithographically fabricated OECTs (Fig. 1). The system was examined using a hardware-in-the-loop configuration based on direct analog signal transfer, in which the raw current output from the sensory module directly drives the downstream axonal oscillator, and the resulting voltage spikes subsequently modulate the synaptic device without any algorithmic scaling or software-based amplification. Functionally, a spiking-generation circuit built from OECTs produces frequency-tunable all-or-none action potentials by exploiting the intrinsic gate capacitance and high transconductance of the device, eliminating the need for external capacitors. A short-term plasticity OECT serves as an artificial synapse, where the postsynaptic current is dynamically modulated by upstream spiking signals. Finally, a light-sensitive OECT acts as the sensory receptor, converting visible-light stimuli directly into current inputs for the neuron. Together, these components form a continuous, physically faithful pathway from the environmental input to synaptic output, demonstrating robust spike generation and downstream plasticity. This study establishes a rigorous experimental foundation for fully integrated, monolithic OECT-based neuromorphic systems and highlights the potential of end-to-end, hardware-implemented organic neurons for flexible, high-density neuromorphic computing.

EXPERIMENTAL

Fabrication of OECTs

OECTs were fabricated on precleaned Si/SiO_2 (300 nm) substrates through a sequential process. First, a negative photoresist (Futurrex NR 99-1500 PY) was spin-coated at 4000 $r\cdot min^{-1}$ for 1 min and subsequently soft baked at 150 °C for 2.5 min. After cooling, ultraviolet exposure was performed through a photomask for 12 s (200–300 W), followed by a post-exposure bake at 120 °C for 2 min. The substrate was then developed in an AZ 300 MIF developer for 45 s, rinsed with deionized water, and hard-baked at 120 °C for 1 min for photolithographic patterning. Subsequently, a Ti/Au (20/80 nm) bilayer was deposited *via* electron-beam evaporation and patterned into the bottom electrodes using a lift-off process in acetone. A 30 nm AlO_x isolation layer was grown by atomic layer deposition (ALD) and patterned *via* the same photolithography steps coupled with wet etching in phosphoric acid at 80 °C for 3.5 min. A 300 nm Ag electrode was then formed on the gate region by thermal evaporation and lift-off lithography; a defined reaction window was opened *via* further lithography, and a 0.5 $mol\cdot L^{-1}$ $FeCl_3$ solution was drop-cast onto the Ag surface. After reacting for 20 min in the dark, a Ag/AgCl gate electrode was obtained. Semiconductor layers were formed by spin-coating at 1000 $r\cdot min^{-1}$ from chloroform solutions of organic semiconductors (5 $mg\cdot mL^{-1}$), followed by patterning *via* lift-off lithography. Finally, a 0.1 $mol\cdot L^{-1}$ KCl aqueous solution was drop-cast onto each channel as the electrolyte, completing the fabrication of all OECT devices. To encapsulate the aqueous KCl electrolyte in the synaptic module, we designed a polydimethylsiloxane (PDMS)-based isolation-well structure. The KCl solution was precisely confined within a PDMS microwell fabricated adjacent to the integrated Ag/AgCl electrode, and a thin PDMS lid was placed on top to form a sealed enclosure.

Characterization of Device Electrical Performance

The electrical performances of the OECT devices and complementary inverters were characterized using a Keithley 4200A-SCS semiconductor parameter analyzer to measure the key electrical properties, including the current-voltage characteristics. The photoelectrical properties of the OECTs were tested using a high-power LED light-source system (Thorlabs) that provided illumination. The performance of the spiking circuits was evaluated using an FS-Pro (PRIMARIUS) semiconductor parameter test system, primarily for assessing electrical behaviors such as voltage–time characteristics.

Signal Transfer in Artificial Neurons

The raw output photocurrents generated by the receptor were converted into positive values using their absolute values, which directly drove the axonal oscillator. The DC offset of the resulting voltage spikes from the artificial axon was removed, and the remaining AC component was inverted and combined with a DC bias (−0.3 V) to modulate the synaptic device, without any algorithmic scaling or software-based amplification.

Implementation of the Hardware-in-the-loop Configuration

The hardware-in-the-loop configuration was realized by directly coupling three OECT-based functional modules: a photosensitive receptor, axon-like spike generation circuit, and synaptic plasticity device. The electrical output of each module physically drove the input of the subsequent stage, establishing a continuous hardware signal pathway from the sensory reception to the synaptic response. Only minimal analog preprocessing was applied during the signal transfer to ensure compatibility between the modules (see above). No algorithmic scaling, digital processing, or software-based amplification was involved. Electrical connections between modules were implemented through direct wiring, whereas measurement instruments were used solely for biasing and signal monitoring. This configuration preserves the native amplitude and temporal characteristics of device-generated signals and enables real-time hardware-level signal propagation across the receptor-axon-synapse pathway.

RESULTS AND DISCUSSION

To realize the functional capabilities of OECT-based artificial neurons, it is first necessary to fabricate high-performance p- and n-type OECTs and subsequently construct complementary inverters. Here, planar-gate OECT devices integrated with Ag/AgCl electrodes were fabricated using standard photolithography (Fig. 2a); the detailed fabrication process is provided in Fig. S1 (in the electronic supplementary information, ESI). We systematically characterized p-type OECTs employing p(g2T-TT) as the hole-transport channel and n-type OECTs using Pg5Tz-5-DPP as the electron-transport channel. Both devices have a channel width-to-length ratio of 400 μm/20 μm and utilize a 0.1 mol·L^{-1} KCl aqueous solution as the electrolyte.

The transfer characteristics of the devices are shown in Figs. 2(b) and 2(c). Under V_{DS} = −0.6 V, the p-type OECT exhibits an on/off ratio (I_{on}/I_{off}) of about 10^6 and a maximum transconductance of 6.29 mS, while the n-type OECT reaches an I_{on}/I_{off} of about 10^5 and a maximum transconductance of 1.62 mS at V_{DS}=0.6 V. The threshold voltages are approximately −0.26 V for the p-type and 0.46 V for the n-type OECTs. The close matching of these values facilitates the construction of complementary inverters with significantly enhanced voltage gain.[24,25] Gate leakage currents (I_G) remain low for both devices, not exceeding 10^{-7} A. Corresponding output characteristics are presented in Figs. 2(d) and 2(e). Together,

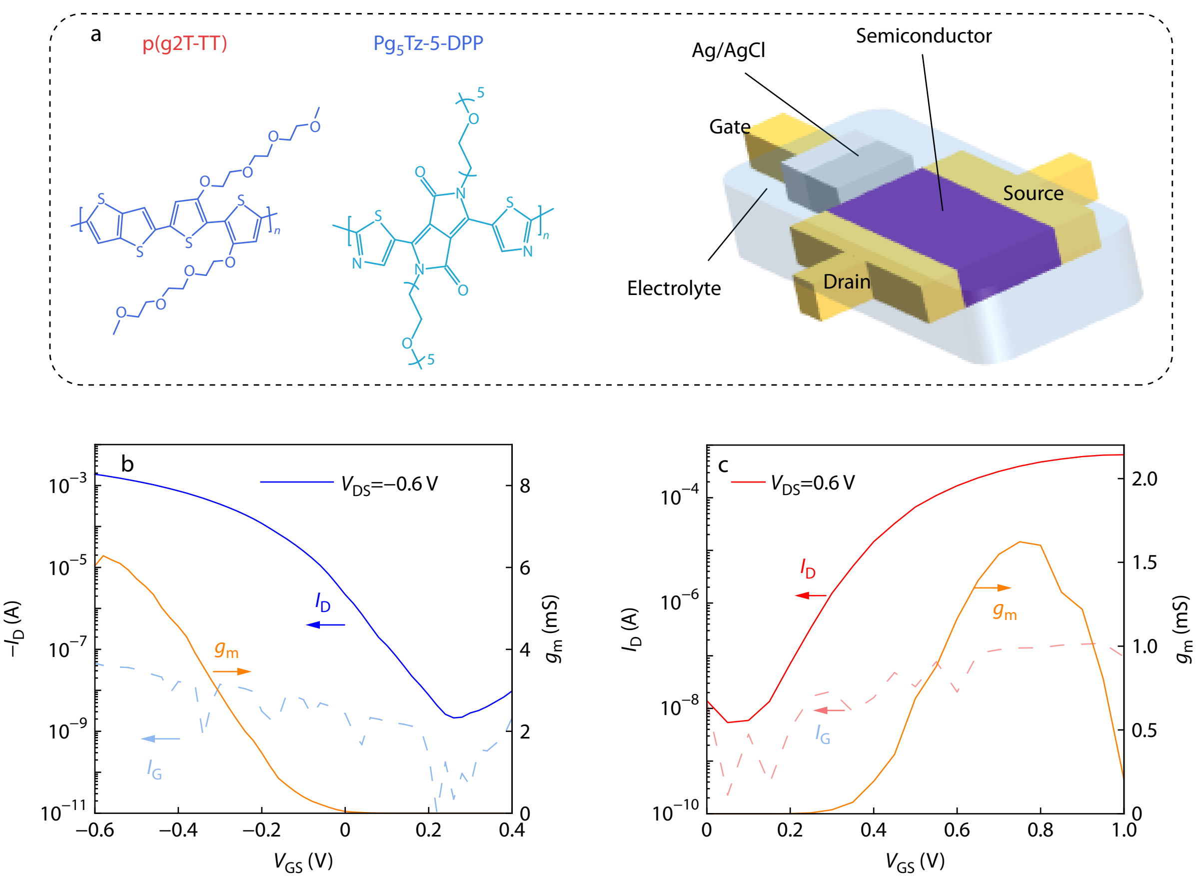

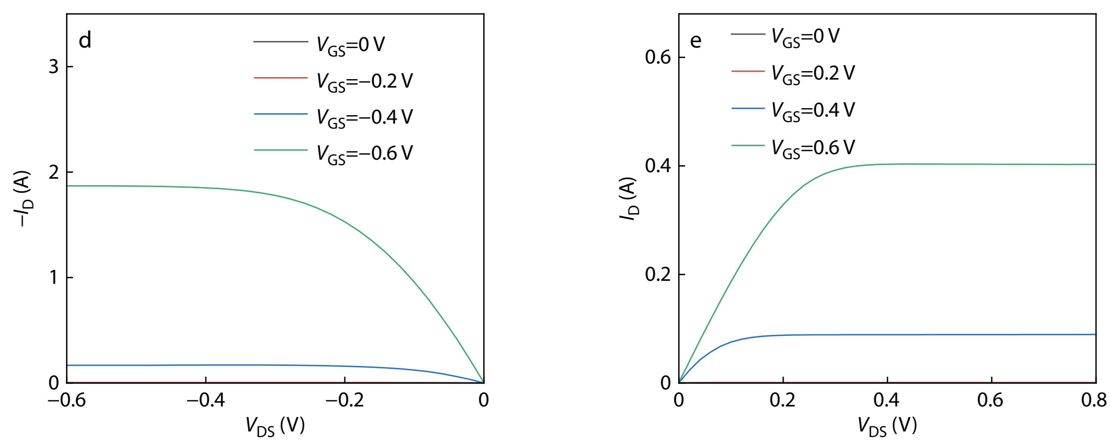

Fig. 2 (a) Schematic diagram of the OECT structure; (b) Transfer and (d) output characteristics of the p-OECT; (c) Transfer and (e) output characteristics of the n-OECT.

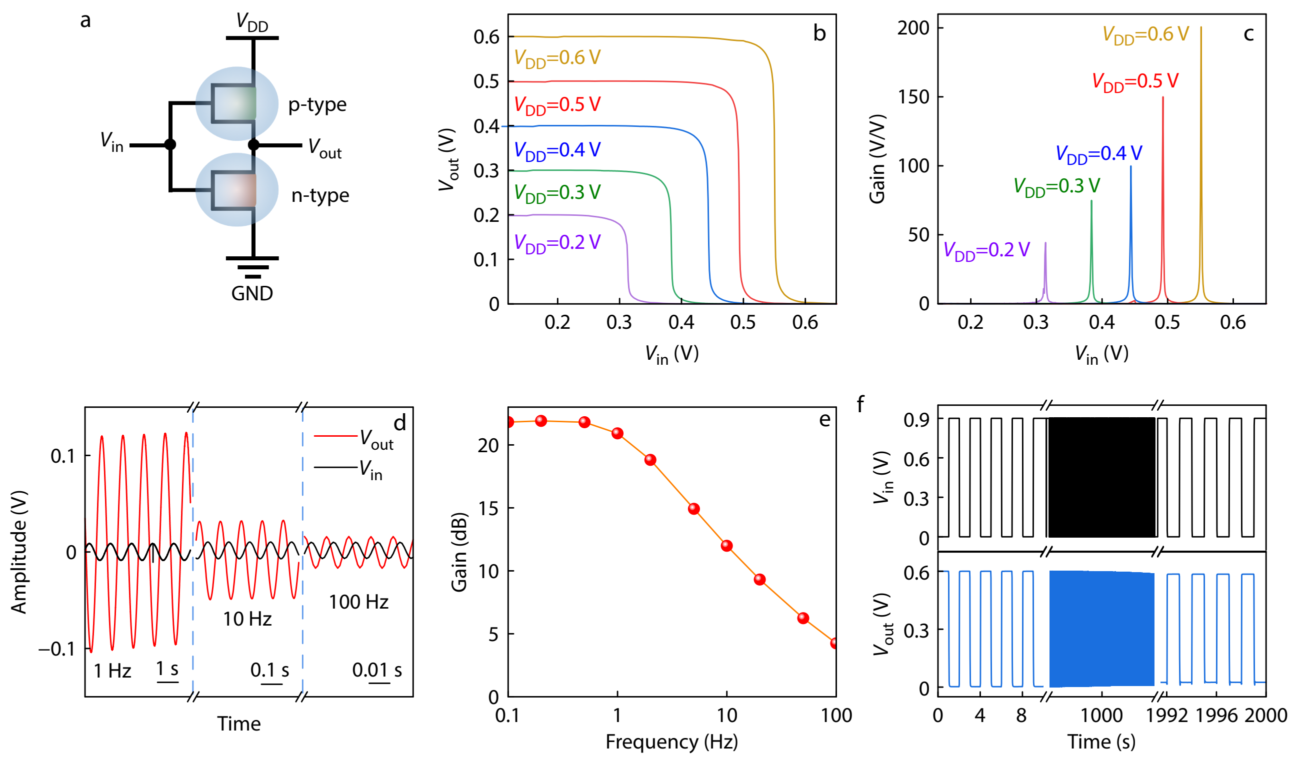

Fig. 3 (a) Schematic diagram of the OECT complementary inverter structure; (b) Transfer characteristics and voltage gain of the complementary inverter; (c) Relationship between the maximum gain and V_{DD}; (d) Amplification of sinusoidal signals at different frequencies by the complementary inverter; (e) Relationship between the amplification factor of sinusoidal signals and frequency for the complementary inverter; (f) Stability of continuous switching of the complementary inverter.

these results demonstrate that the fabricated OECTs exhibit excellent electrical performance, providing a robust foundation for high-gain inverter design and subsequent implementation of spike-generation circuits.

Complementary inverters (Fig. 3a) outperform unipolar designs by substantially reducing static power consumption. In each logic state, one transistor is off, creating a high-impedance path between the supply rails, which enables a full rail-to-rail output swing, enhanced noise margins (NM), and improved energy efficiency.[26,27] Fig. 3(b) shows the voltage transfer characteristics and the corresponding gain of the OECT-based complementary inverter under varying supply voltages (V_{DD}). Both the switching threshold and gain are tunable with V_{DD}, and at V_{DD}=0.6 V, the voltage gain reaches 201 V/V, which represents the state-of-the-art performance among OECT-based inverters (Table S1 in ESI). The maximum gain values for each V_{DD} are shown in Fig. 3(c), highlighting the potential of the inverter for low-amplitude analog signal processing. Because one OECT is fully on (low resistance) and the other is fully off (high resistance), the output is pulled directly to the supply rail with minimal voltage loss from the channel conduction (less than 0.01 V). NM values are also

https://doi.org/10.1007/s10118-026-3703-9

evaluated (Fig. S2 in ESI), thereby demonstrating robust noise immunity and reliable logic discrimination across a wide input range.[25,28] Comparative performance metrics for the NM relative to previous studies are summarized in Table S2 (in ESI), further illustrating the competitive advantage of our fabricated complementary inverters.

To assess the amplification performance of the inverter across the typical low-frequency range of bioelectrical signals (0.1–100 Hz), the device was biased at its maximum-gain point to ensure optimal sensitivity.[29,30] A sinusoidal input with a peak-to-peak amplitude of 20 mV, representative of physiological signal magnitudes, was applied for frequency response characterization. As shown in Fig. 3(d), the output waveforms at 1 , 10 , and 100 Hz exhibit both clear amplification and excellent temporal fidelity, demonstrating that the circuit preserves signal integrity while providing consistent gain across the tested spectrum. The voltage-gain-frequency relationship (Fig. 3e) reveals a stable amplification plateau throughout the low-frequency band, confirming its suitability for steady and slowly varying bioelectrical signals such as electrocardiograms (ECG) and electroencephalograms (EEG).[31] Low output distortion and consistent gain underscore the reliability of the inverter as a signal-conditioning module for wearable or implantable biomedical systems. The performance uniformity across the devices is shown in Fig. S3 (in ESI), which reports the maximum gain and noise margin for the 11 complementary inverters. In the repeatability tests, the inverter maintains stable operation over 1000 consecutive switching cycles (Fig. 3f), demonstrating excellent durability. Power analysis (Fig. S4 in ESI) confirms ultralow consumption (10^{-8}–10^{-9} W), a direct consequence of the complementary architecture, which minimizes quiescent current and

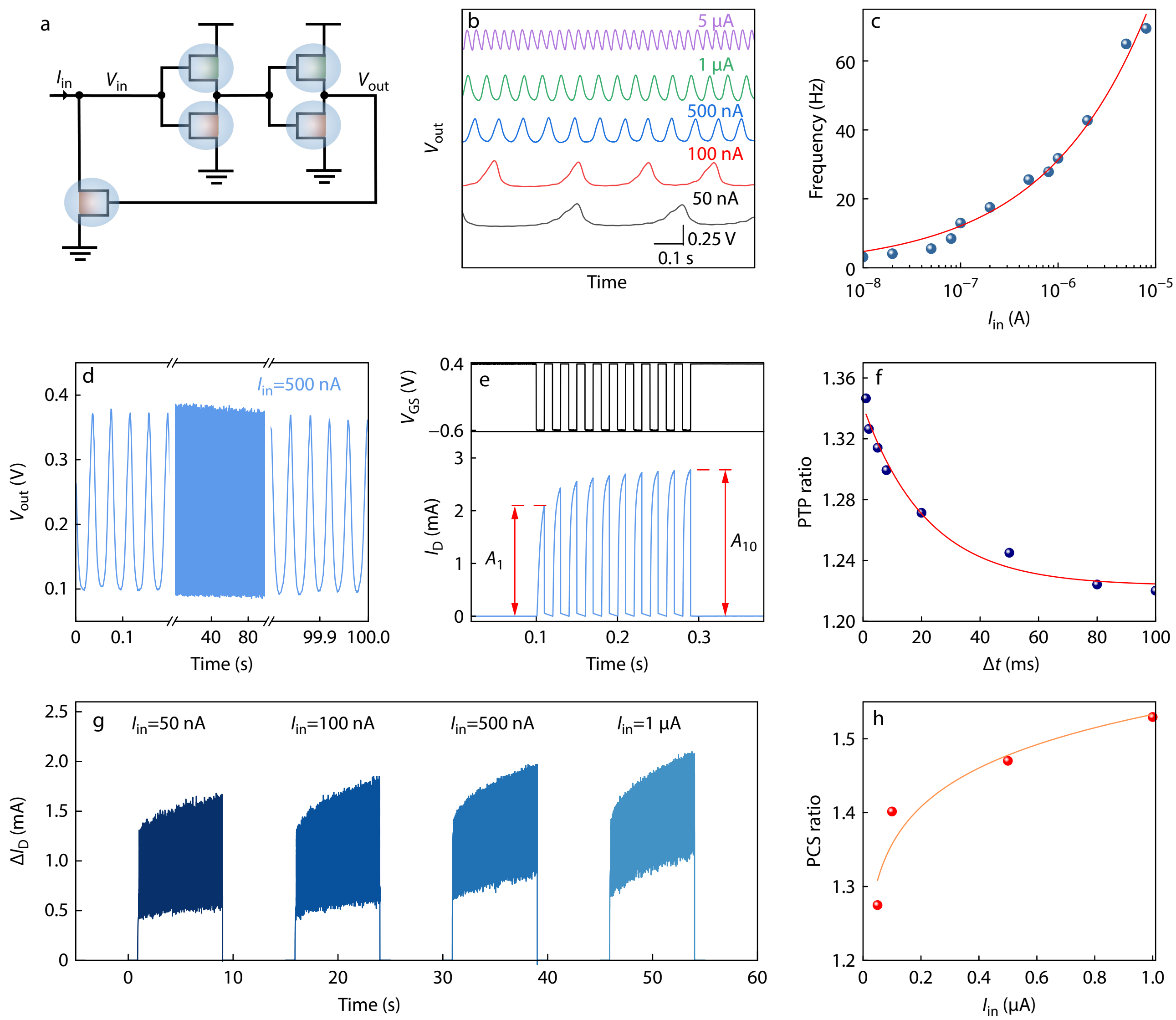

Fig. 4 (a) Schematic diagram of the Axon-Hillock circuit; (b) Output spike signals under different I_{in}; (c) Relationship between spike signal frequency and I_{in}; (d) Output results of the spike generation circuit under continuous operation for 100 s; (e) Current response of the OECT synaptic device to ten square-wave pulses; (f) PTP index and pulse interval; (g) Response of the OECT synaptic device to spike signals; (h) Relationship between the PCS index and spike input current.

ensures energy is primarily expended during active signal amplification.[32]

Biological neurons generate action potentials when membrane potential exceeds a well-defined threshold. To emulate this behavior, we adopted an axon hillock-inspired circuit architecture (Fig. 4a in ESI). The circuit consists of two stages of complementary inverters configured as high-gain non-inverting amplifiers, together with an n-type OECT acting as a reset transistor, forming a compact spike-generation module. During operation, the input direct current (I_{in}) charges the intrinsic parasitic capacitance of the circuit, leading to a gradual increase in the input voltage (V_{in}). Once V_{in} exceeds the switching threshold of the inverters, the high-gain amplifier produces a rapid increase in output voltage (V_{out}). This increase in V_{out} activates the reset transistor, creating a discharge pathway that rapidly reduces V_{in}. The resulting drop in V_{in} causes V_{out} to fall and turns off the reset transistor, thereby completing a single-spike event. The charging process then resumed under the applied I_{in}, initiating the next spiking cycle. By varying the magnitude of I_{in}, the capacitance charging rate is continuously tuned by varying the magnitude of I_{in}, enabling precise control over the output spike frequency.[5]

The performances of the two cascaded complementary inverters are shown in Fig. S5 (in ESI). The resulting voltage transfer characteristic exhibits a sharp rail-to-rail transition with a near-ideal gain, confirming efficient signal propagation. Importantly, the measured NM shows no degradation relative to that of a single inverter, indicating that the cascaded architecture amplifies the signal while preserving intrinsic robustness against voltage fluctuations, which is an essential requirement for reliable operation in noisy physiological environments. As shown in Fig. 4(b), the spike signals at V_{out} under the same I_{in} demonstrate that, within a defined current window, the spike frequency can be continuously tuned, spanning the low-frequency regime characteristic of biological neural activity. This behavior highlights the suitability of this circuit for biocompatible neuromorphic applications.[31] For example, increasing I_{in} from 50 nA to 5 μA raises the output frequency from 5.56 Hz to 64.9 Hz, effectively covering the physiological range of neuronal firing rates. Fig. 4(c) further shows the relationship between output frequency and I_{in}, thereby confirming the predictable and scalable frequency modulation capability of the circuit over the tested input range. Additionally, when operated at I_{in}=50 nA, the circuit exhibits stable spiking behavior over continuous operation for 100 s (Fig. 4d) and remained fully functional after storage in a nitrogen environment for seven days (Fig. S6 in ESI), thereby demonstrating robust short-term operational stability.

Notably, the p-type OECT shown in Figs. 2(b) and 2(d) can function as the synaptic element of the artificial neuron. The device effectively emulates short-term synaptic plasticity, exhibiting two hallmark memory behaviors of biological synapses: paired-pulse facilitation (PPF) and post-tetanic potentiation (PTP). These responses constitute key biomimetic features of synaptic information processing. As shown in Fig. 4(e) and Fig. S7 (in ESI), under pulsed stimulation with varying interpulse intervals, the postsynaptic current displays pronounced facilitation, reflecting a clear dependence on the stimulation history. To further examine the accumulation characteristics of short-term plasticity, sequences of voltage pulses with varying pulse numbers were applied to the synaptic module, while monitoring the corresponding postsynaptic current (PSC) amplitude. As shown in Fig. S8 (in ESI), the PSC progressively increases with pulse number, indicating pronounced short-term plasticity accumulation. This pulse-number-dependent facilitation demonstrates the capability of the device to integrate temporally correlated stimuli, which is a key functionality for dynamic information processing in neuromorphic systems. This behavior closely mirrors the temporally dependent plasticity mechanisms observed in biological synapses. Furthermore, as shown in Fig. 4(f), the current gain exhibits strong interval dependence, enabling dynamic signal integration and a sustained post-tetanic response following high-frequency stimulation.

To evaluate the signal compatibility and cooperative operation between the axon zone (spiking circuit) and synaptic zone, the output signal of the spiking circuit was directly interfaced with the synaptic device after a minimal preprocessing step that faithfully preserved the native spike amplitude and temporal characteristics. This procedure closely mimics the transmission of biological spikes from the axon to synapse. As shown in Fig. 4(g), the synaptic device reliably receives spike trains generated under different axons, I_{in} and converts them into distinct postsynaptic current responses. When the spiking input current was 50 nA, the postsynaptic current enhancement factor was 1.27, which increases to 1.53 as I_{in} increased to 1 μA. Moreover, as quantitatively summarized in Fig. 4(h), the postsynaptic current amplitude was systematically modulated by I_{in}, demonstrating a clear and monotonic coupling between the two functional zones. These results confirm that spike signals generated by the axon circuit can directly and effectively regulate synaptic response strength without auxiliary signal conditioning, thereby validating the feasibility and robustness of the integrated two-stage system comprising axon and synaptic zones for reliable signal transmission and cooperative neuromorphic processing.

To realize an artificial neuron with end-to-end sensory perception and information processing capabilities, we selected a p-type OECT based on a photosensitive polymer (R6, Fig. S9 in ESI) as the signal-reception module. The transfer and output characteristics of this device are shown in Figs. 5(a) and 5(b), respectively, demonstrating pronounced photosensitivity under illumination at specific wavelengths. As illustrated in Fig. 5(c), the real-time photoresponse reaches 48.5 nA at V_{GS}=−0.1 V and increases to 65.8 nA at V_{GS}=−0.2 V. From the transient photoresponse curves at V_{GS}=−0.2 V (Fig. 5c), the rise time (defined as the time for the photocurrent to increase from 10% to 90% of the peak value) and fall time (from 90% to 10% of the peak value) are measured to be approximately 6.40 and 7.15 s, respectively. We further characterized the light-intensity dependence of the photosensitive OECT by measuring its photocurrent output under varying illumination intensities. It is clear that the photocurrent increases monotonically with increasing light intensity (Fig. S10a in ESI). The spectral response range of the photosensitive OECT was evaluated by measuring the photocurrent under monochro-

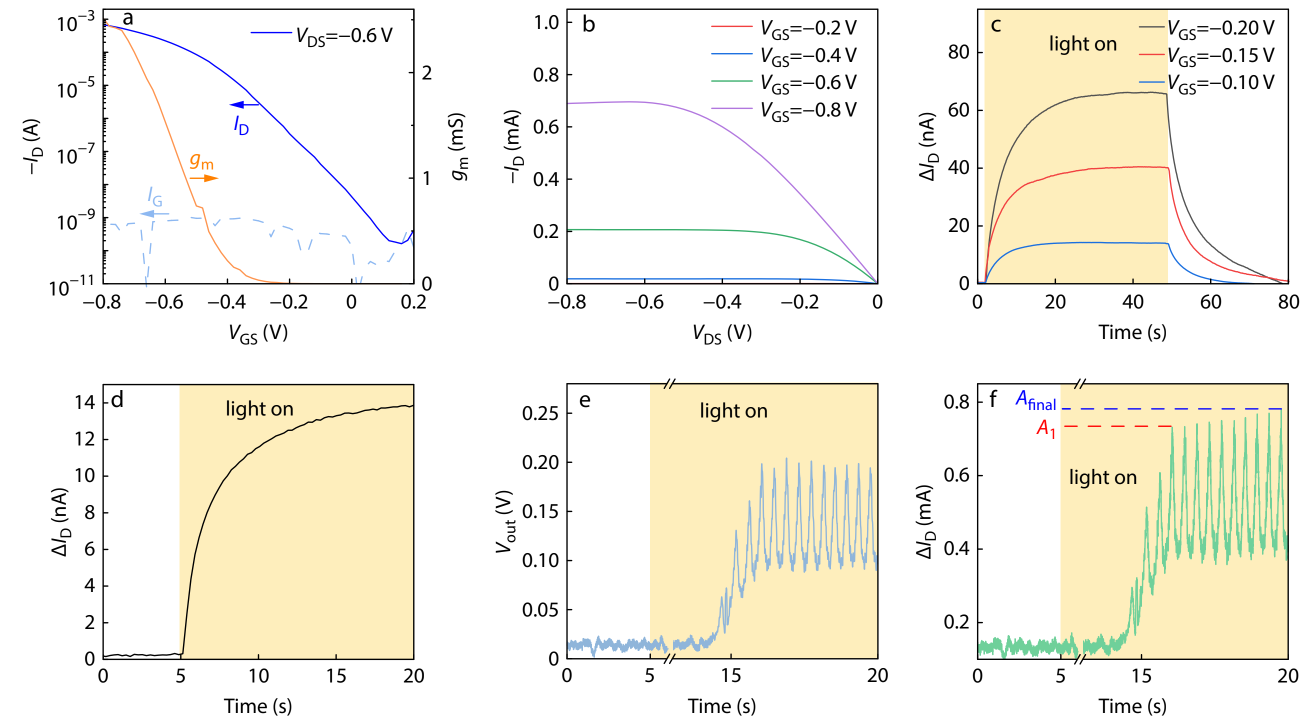

Fig. 5 (a) Transfer characteristic curve of the photo-responsive OECT; (b) Output characteristics of the photo-responsive OECT; (c) Photocurrent response of the OECT; (d) Photocurrent response, (e) spike signals, and (f) synaptic current response of the complete artificial neuron.

matic light irradiation at different wavelengths (Fig. S10b in ESI). A higher V_{GS} drives the OECT into a high transconductance regime, where the drain current becomes highly sensitive to carrier density variations. Consequently, photogenerated carriers induce a larger conductivity modulation, resulting in an enhanced photocurrent response.[33] By incorporating this photosensitive OECT as the signal reception zone and interfacing it with the previously established axon and synapse zones, a complete neuron-inspired signal transduction chain comprising reception, spike generation, and synaptic processing is constructed. In this configuration, the photocurrent generated by the photoreceptor is directly used as the input to the axon zone, where it is converted into spike trains, and the resulting spiking output is subsequently delivered to the synaptic zone to modulate the synaptic plasticity. Specifically, the photocurrent generated at V_{GS}= −0.09 V (Fig. 5d) serves as the driving signal for the OECT-based spiking circuit and downstream synaptic device.

Under optical stimulation, the axon circuit produces corresponding spike outputs (Fig. 5e), which in turn induce potentiation of the postsynaptic current in the synaptic zone (Fig. 5f). The postsynaptic current increases from an initial amplitude (A_1) of 0.73 mA to a final amplitude (A_{final}) of 0.78 mA, corresponding to a potentiation ratio A_{final}/A_1 of 1.07. When the input photocurrent falls below a threshold level, no spike generation is observed, primarily due to leakage currents inherent to the devices, which is consistent with threshold-dependent firing behavior in biological neurons.[34] Together, these results demonstrate a fully functional end-to-end neuron-inspired system, in which external optical stimuli are sensed by a photoreceptive OECT, transformed into spike-encoded signals by an axon-like circuit, and ultimately translated into adaptive synaptic responses. This integrated organic electrochemical neuron unifies sensing, encoding, transmission, and short-term plasticity within a single hardware framework, closely emulating the biological sequence from receptor activation to synaptic information processing. This approach provides a device-level pathway for neuromorphic sensing systems capable of direct environmental interaction and adaptive signal processing.

CONCLUSIONS

In conclusion, we demonstrated a fully lithography-defined neuromorphic neuron architecture that achieves end-to-end neuron-inspired signal transduction using OECT devices. High-performance p- and n-type OECTs enable complementary inverters with voltage gains exceeding 200 V/V, forming the basis for an Axon-Hillock-inspired spiking circuit that generates stable, continuously tunable all-or-none spikes within biologically relevant frequency ranges. By integrating a p-type OECT-based synapse exhibiting short-term plasticity and a photosensitive OECT serving as the signal-reception zone, the system realizes a complete hardware neural pathway from sensory perception to spike-based transmission and synaptic modulation. Importantly, signal propagation across the receptor, axon, and synapse zones is achieved through direct analog coupling without external discrete components or algorithmic scaling or amplification, highlighting the intrinsic electrical compatibility of OECT-based functional blocks. In the present proof-of-concept demonstration, the three functional modules are arranged in a planar configuration and interconnected through wired connections, enabling the independent verification of each functional block and reliable signal transfer between them. This work establishes a compact and scalable platform for neuromorphic perception hardware, and the lithography-defined device architecture further provides a pathway toward dense integration using standard microfabrication technologies, offering a device-level route toward adaptive bioinspired systems capable of direct interaction with complex environments.

The ultimate goal of neuromorphic systems is to realize direct functional coupling across the full neuronal pathway from perception to transmission and short-term memory, such that stimulation of the sensory unit can immediately elicit synaptic plasticity without external encoding or relay circuits.[34,35] Achieving this level of integration is currently limited by signal-interface mismatches; sensory OECTs typically produce slowly varying analog outputs, whereas spiking and synaptic modulation require well-defined voltage amplitudes, temporal profiles, and thresholds.[2,6] Overcoming this bottleneck will require coordinated advances across materials, devices, and circuits. At the material level, multimodal-responsive organic semiconductors may enable sensory outputs that intrinsically match synaptic modulation requirements.[36,37] At the device level, multifunctional OECT architectures integrating sensing and nonlinear preprocessing could serve as compact "sensing-processing" units.[38] At the circuit level, leveraging intrinsic OECT properties, such as anti-ambipolarity, may further simplify spike generation and reduce system complexity.[6,39] In parallel, future system integration may transition from the present planar prototype toward monolithic interconnections on flexible substrates, where different functional modules are directly linked through microfabricated metal interconnects. Multilayer architectures with vertical interconnects can further reduce the footprint by stacking sensory, processing, and synaptic layers. Together, these directions outline a path toward fully integrated organic neuromorphic hardware with physically coupled perception, transmission, and plasticity, while the inherent scalability of OECT devices, whose channel dimensions can be reduced to micrometer or even sub-micrometer scales using standard microfabrication, supports high-density integration suitable for wearable and adaptive sensing systems.

Conflict of Interests

The authors declare no interest conflict.

Electronic Supplementary Information

Electronic supplementary information (ESI) is available free of charge in the online version of this article at http://doi.org/10.1007/s10118-026-3703-9.

Data Availability Statement

The related data of this paper is data that should not be shared, and can be obtained from the author for reasonable reasons. The author's contact information: limengmeng@ucas.ac.cn.

ACKNOWLEDGMENTS

This work was financially supported by the National Key R&D Program of China (No. 2025YFF0518300), the Beijing Natural Science Foundation (No. JQ24030), the National Natural Science Foundation of China (No. U25A20481), the Fundamental Research Funds for the Central Universities, and the Self-deployment Project of the State Key Laboratory of Fabrication

Graphical Abstract

End-to-End Neuron-inspired Signal Transduction Using Organic Electrochemical Transistors

Jin-Yao Wang, Yue Tian, Yi-Fan Xie, Miao Cheng, Chang-Rui Liu, Jing-Yun Chu, Guo-Qing Xie, Neng Gao, Hao-Fan He, Le-Jing Huang, Ling-Fei Wang, and Meng-Meng Li

Institute of Microelectronics, Chinese Academy of Sciences; University of Chinese Academy of Sciences; State Key Laboratory of Fabrication Technologies for Integrated Circuits, Chinese Academy of Sciences

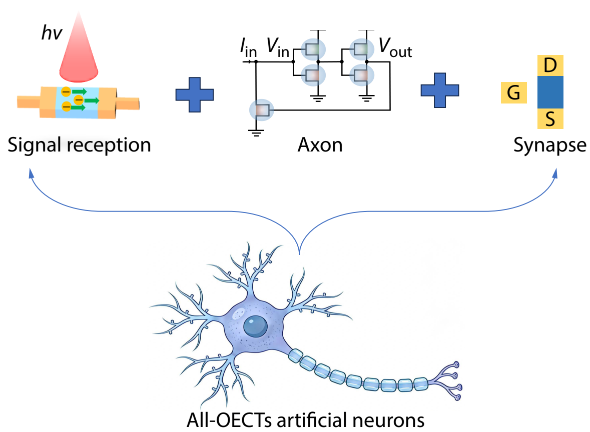

This work demonstrates an end-to-end neuron-inspired signal pathway built entirely from organic electrochemical transistors (OECTs), where a photosensitive receptor directly drives axonal spiking and synaptic plasticity through analog hardware coupling without algorithmic processing.

Chinese J. Polym. Sci., 2026 *https://doi.org/10.1007/s10118-026-3703-9*

Technologies for Integrated Circuits.

REFERENCES

1 Boufidis, D.; Garg, R.; Angelopoulos, E.; Cullen, D. K.; Vitale, F. Bio-inspired electronics: soft, biohybrid, and "living" neural interfaces. *Nat. Commun.* **2025**, *16*, 1861.

2 Harikesh, P. C.; Tu, D.; Fabiano, S. Organic electrochemical neurons for neuromorphic perception. *Nature Electronics* **2024**, *7*, 525–536.

3 van de Burgt, Y.; Lubberman, E.; Fuller, E. J.; Keene, S. T.; Faria, G. C.; Agarwal, S.; Marinella, M. J.; Alec Talin, A.; Salleo, A. A non-volatile organic electrochemical device as a low-voltage artificial synapse for neuromorphic computing. *Nat. Mater.* **2017**, *16*, 414–418.

4 Ro, Y. G.; Chang, Y.; Kim, J.; Lee, S.; Na, S.; Park, C.; Ko, H. Ionic–bionic interfaces: Advancing iontronic strategies for bioelectronic sensing and therapy. *Adv. Sci.* **2025**, *13*, e13985.

5 Harikesh, P. C.; Yang, C. Y.; Tu, D.; Gerasimov, J. Y.; Dar, A. M.; Armada-Moreira, A.; Massetti, M.; Kroon, R.; Bliman, D.; Olsson, R.; Stavrinidou, E.; Berggren, M.; Fabiano, S. Organic electrochemical neurons and synapses with ion mediated spiking. *Nat. Commun.* **2022**, *13*, 901.

6 Ji, J.; Gao, D.; Wu, H.-Y.; Xiong, M.; Stajkovic, N.; Latte Bovio, C.; Yang, C.-Y.; Santoro, F.; Tu, D.; Fabiano, S. Single-transistor organic electrochemical neurons. *Nat. Commun.* **2025**, *16*, 4334.

7 Xia, Y.; Zhang, C.; Xu, Z.; Lu, S.; Cheng, X.; Wei, S.; Yuan, J.; Sun, Y.; Li, Y. Organic iontronic memristors for artificial synapses and bionic neuromorphic computing. *Nanoscale* **2024**, *16*, 1471–1489.

8 Cheng, W.; Zhu, Y.; Jiang, G.; Cao, K.; Zeng, S.; Chen, W.; Zhao, D.; Yu, H. Sustainable cellulose and its derivatives for promising biomedical applications. *Prog. Mater Sci.* **2023**, *138*, 101152.

9 Rivnay, J.; Inal, S.; Salleo, A.; Owens, R. M.; Berggren, M.; Malliaras, G. G. Organic electrochemical transistors. *Nat. Rev. Mater.* **2018**, *3*, 17086.

10 Khodagholy, D.; Rivnay, J.; Sessolo, M.; Gurfinkel, M.; Leleux, P.; Jimison, L. H.; Stavrinidou, E.; Herve, T.; Sanaur, S.; Owens, R. M.; Malliaras, G. G. High transconductance organic electrochemical transistors. *Nat Commun* **2013**, *4*, 2133.

11 Li, L.; Chen, W.; Kong, X.-Y.; Wen, L. Nanofluidic neuromorphic iontronics: a nexus for biological signal transduction. *Iontronics* **2026**, *2*, 4.

12 Li, Y.; Su, K.; Chen, H.; Zou, X.; Wang, C.; Man, H.; Liu, K.; Xi, X.; Li, T. Research progress of neural synapses based on memristors. *Electronics* **2023**, *12*, 3298.

13 Indiveri, G.; Liu, S. C. Memory and information processing in neuromorphic systems. *Proc. IEEE* **2015**, *103*, 1379–1397.

14 Mead, C. Neuromorphic electronic systems. *Proc. IEEE* **1990**, *78*, 1629–1636.

15 Yao, Y.; Pankow, R. M.; Huang, W.; Wu, C.; Gao, L.; Cho, Y.; Chen, J.; Zhang, D.; Sharma, S.; Liu, X.; Wang, Y.; Peng, B.; Chung, S.; Cho, K.; Fabiano, S.; Ye, Z.; Ping, J.; Marks, T. J.; Facchetti, A. An organic electrochemical neuron for a neuromorphic perception system. *PNAS* **2025**, *122*, e2414879122.

16 Pickett, M. D.; Stanley Williams, R. Sub-100 fj and sub-nanosecond thermally driven threshold switching in niobium oxide crosspoint nanodevices. *Nanotechnology* **2012**, *23*, 215202.

17 Wang, L.; Jiao, Y.; Zhang, H.; Liu, Y.; Zhang, Y.; Wu, P.; Xiao, K. Neuromorphic iontronic devices based on soft ionic conductors. *Chem. Soc. Rev.* **2026**, *55*, 299–335.

18 Chua, L. Memristor, hodgkin–huxley, and edge of chaos. *Nanotechnology* **2013**, *24*, 383001.

19 Yang, J. J.; Strukov, D. B.; Stewart, D. R. Memristive devices for computing. *Nat. Nanotechnol.* **2013**, *8*, 13–24.

20 Wang, Y.; Shan, W.; Li, H.; Lei, X.; Chang, T.; El-Atab, N.; Lei, T.; Inal, S. A retina-inspired organic iono-optoelectronic synapse. *Adv Mater* **2025,** e14620.

21 Laswick, Z.; Wu, X.; Surendran, A.; Zhou, Z.; Ji, X.; Matrone, G. M.; Leong, W. L.; Rivnay, J. Tunable anti-ambipolar vertical bilayer organic electrochemical transistor enable neuromorphic retinal pathway. *Nat. Commun.* **2024**, *15*, 6309.

22 Kim, D.-H.; Lee, J.; Kim, Y.; Yoo, H.; Lee, E. K. Enhanced synaptic behavior of neuromorphic device based on organic electrochemical transistors by adding aminosilane. *Org. Electron.* **2024**, *131*, 107076.

23 Bisquert, J.; Tessler, N. A one-transistor organic electrochemical self-sustained oscillator model for neuromorphic networks. *Newton* **2025**, *1*, 100207.

24 Kuang, Y.; Yao, T.; Deng, S.; Dong, J.; Ye, G.; Zhang, L.; Shao, S.; Zhu, Z.; Liu, J.; Liu, J. Matching p- and n-type organic electrochemical transistor performance enables a record high-gain complementary inverter. *Adv Mater* **2025**, *37*, e2417691.

25 Zhou, Z.; He, Q.; Tang, C. G.; Hou, K.; Yang, J.; Kousseff, C. J.; McCulloch, I.; Leong, W. L. Multifunctional electronics enabled by ion-based organic electrochemical transistor with large threshold voltage tunability window. *ACS Nano* **2025**, *19*, 37865–37878.

26 Yadav, Y.; Singh, S. P. Ionic liquid gated unipolar inverters with tunable switching voltage and excellent noise margin. *J. Mater. Chem. C* **2023**, *11*, 1021–1028.

27 Takeda, Y.; Hayasaka, K.; Shiwaku, R.; Yokosawa, K.; Shiba, T.; Mamada, M.; Kumaki, D.; Fukuda, K.; Tokito, S. Fabrication of ultra-thin printed organic tft cmos logic circuits optimized for low-voltage wearable sensor applications. *Sci. Rep.* **2016**, *6*, 25714.

28 Travaglini, L.; Fidanovski, K.; Mawad, D. Logic circuits featuring organic electrochemical transistors: what is the logic behind oects in logic. *Adv. Sci*. **2025,** *12*, e14448.

29 Lu, D.; Chen, H. Solid-state organic electrochemical transistors (oects) based on gel electrolytes for biosensors and bioelectronics. *J. Mater. Chem. A* **2025**, *13*, 136–157.

30 Zhu, Z.; Wang, X.; Wang, D.; Gu, Y.; Fan, W.; Pang, Y.; Guo, Z.; Li, Y. Fine-grained ecg monitoring based on stretchable organic electrochemical transistors with anisotropic gel electrolytes for biometric identification. *ACS Sens* **2025**, *10*, 9423–9431.

31 Tian, Z.; Zhao, Z.; Yan, F. Organic electrochemical transistor in wearable bioelectronics: profiles, applications, and integration. *Wear. Electron.* **2024**, *1*, 1–25.

32 Huang, W.; Chen, J.; Yao, Y.; Zheng, D.; Ji, X.; Feng, L.-W.; Moore, D.; Glavin, N. R.; Xie, M.; Chen, Y.; Pankow, R. M.; Surendran, A.; Wang, Z.; Xia, Y.; Bai, L.; Rivnay, J.; Ping, J.; Guo, X.; Cheng, Y.; Marks, T. J.; Facchetti, A. Vertical organic electrochemical transistors for complementary circuits. *Nature* **2023**, *613*, 496–502.

33 Zhong, Y.; Koklu, A.; Villalva, D. R.; Zhang, Y.; Hernandez, L. H.; Moser, M.; Hallani, R. K.; McCulloch, I.; Baran, D.; Inal, S. An organic electrochemical transistor integrated photodetector for high quality photoplethysmogram signal acquisition. *Adv. Funct. Mater.* **2023**, *33*, 2211479.

34 Sun, S.; You, Z.; Ji, Y.; Li, Y.; Feng, Y.; Liu, S.; Cao, J.; Liu, Y.; Yu, Z.; Wu, T. Application and challenges of organic electrochemical

transistors in neuromorphic computing: bionic synapse and multi-mode integration. *J. Mater. Chem. C* **2025**, *13*, 19125−19148.

35 van de Burgt, Y.; Melianas, A.; Keene, S. T.; Malliaras, G.; Salleo, A. Organic electronics for neuromorphic computing. *Nat. Electron.* **2018**, *1*, 386−397.

36 Lei, P.; He, Z.; Cao, L.; Zhang, M.; Zheng, C.; Lin, H.; Du, X.; Tao, S. Multifunctional organic artificial optoelectronic synapses for neuromorphic computing and a weak-light-sensitive visual system. *J. Mater. Chem. C* **2025**, *13*, 11707−11717.

37 Mao, Y.; Choi, Y.; Qian, C.; Roe, D. G.; Kim, S.; Liu, Y.; Chen, D.; Tang, D.; Sun, J.; Cho, J. H. Multimodal in-sensor computing with dual-phase organic synapses for wearable fitness monitoring. *Adv. Mater.* **2026**, *38*, e13904.

38 Xiang, K.; Song, J.; Liu, H.; Chen, J.; Yan, F. Organic electrochemical transistors for neuromorphic devices and applications. *Adv. Mater.* **2025**, *13*, e15532.

39 Sarkar, T.; Lieberth, K.; Pavlou, A.; Frank, T.; Mailaender, V.; McCulloch, I.; Blom, P. W. M.; Torricelli, F.; Gkoupidenis, P. An organic artificial spiking neuron for in situ neuromorphic sensing and biointerfacing. *Nat. Electron.* **2022**, *5*, 774−783.

https://doi.org/10.1007/s10118-026-3703-9